EXPERIMENTAL AND NUMERICAL STUDY
OF A RADIAL FLOW PUMP IMPELLER
WITH 2D-CURVED BLADES

VASILIOS A. GRAPSAS, JOHN S. ANAGNOSTOPOULOS AND DIMITRIOS E. PAPANTONIS
Laboratory of Hydraulic Turbomachines
School of Mechanical Engineering / Fluids Section
National Technical University of Athens
Heroon Polytechniou 9, Zografou, 15780 Athens,
GREECE

Abstract: The present paper describes an experimental and numerical investigation of a radial flow pump impeller with 2D curvature blade geometry. Investigation of the behavior of the above impeller for a wide flow rate range and for various rotational speeds was carried out and the obtained experimental results were validated with available measurements of the same impeller within spiral casing. The flow field through the impeller was also simulated by a 2-dimensional approach. For the numerical simulation, the viscous Navier-Stokes equations are solved with the control volume approach and the k-ε turbulence model. The flow domain is discretized with a polar, unstructured, Cartesian mesh that covers a periodically symmetric section of the impeller. Advanced numerical techniques for adaptive grid refinement and for the partially blocked cells are also implemented at the irregular boundaries of the blades. The numerical results are compared to the measurements, showing good agreement and encouraging the extension of the developed computation methodology for performance prediction and for design optimization of such impeller geometries.

Key-Words: Centrifugal pump impeller; Pump laboratory model; numerical simulation; unstructured Cartesian grid; characteristic curves measurements.

1   Introduction

The increasing performance levels and operating conditions requirements make the task of designing a pump impeller very challenging. The role of internal flows and the viscous effects in centrifugal impellers are fundamental and must be taken properly into account in the design process in order to obtain optimum performance. Formerly it was sufficient for a designer to analyze the steady state operation of a pumping system but nowadays with the increasing complexity of pumping systems, experimental and numerical analysis is desirable [1, 2]. However, detailed experimental investigation can be performed for only simple flows and any empirical generalization to 3D geometries is mostly erroneous. On the other hand, Computational Fluid Dynamics (CFD) analysis and the numerical simulation of the flow has become a requisite tool for the design of hydraulic turbomachinery especially of complex geometries where the experimental approach is time consuming and exhibits some difficulties.

Not many CFD studies or measurements concerning the complex flow in all types of centrifugal pumps have been reported [3, 4]. In order to generate a uniform circumferential pressure distribution at the impeller outlet and simplify the flow field, Sinha and Katz have recently presented an experimental apparatus with the impeller inserted to a shroud-sided casing made of plexiglass [5]. In 2002, Friedrichs and Kosyna [6] used such a test facility, with a vaneless radial diffuser instead of a volute, in order to study a matter of special interest, such as the rotating cavitation in a centrifugal pump impeller of low specific speed. Based on this approach, Furukawa et al. [7] studied the pressure fluctuation in a vaned diffuser downstream from a centrifugal pump impeller.

In this context, the present work combines an experimental and a numerical investigation of a centrifugal pump. The experimental survey was conducted on a radial flow pump impeller, with single circular arc blades, for different discharge valve settings and for various rotation speeds. For the validation of the measurements available measurements of the same impeller within a spiral case were used [8]. The numerical simulation of the flow in the 2D radial flow pump impeller is conducted with an advanced numerical algorithm, which has been recently used in similar geometries

with encouraging results [9, 10]. The predicted results for the characteristic curves are presented over the entire flow range and were compared to the experimental ones.

2   Experimental Apparatus

2.1   Test Facility

Figure 1 shows a cross-sectional view of the experimental test section, with a vertical rotating shaft, which was constructed and installed in the Laboratory of Hydraulic Turbomachinery of NTUA. Flowing into the impeller from an open tank, through a suction pipe, water is discharged to a parallel walled diffuser with a height of 90mm (which is the same with the impeller blade exit width) and it returns through twelve uniformly distributed pipes to the tank. So the formed casing is axisymmetric and the generated flow field exhibits periodic symmetry. The diffuser and the casing are made of plexiglass to enable direct observations of the flow.

The measuring equipment is composed by two differential pressure transducers, one measuring the head of the pump (by measuring the pressure difference in points "1" and "2", Fig. 1) and the second measuring the flow rate (through the pressure difference across a calibrated orifice plate), a torsional torque meter installed at the shaft between the impeller and the motor, and a digital counter for the speed of rotation. The experimental setup with the instrumentation system is shown in Fig. 2.
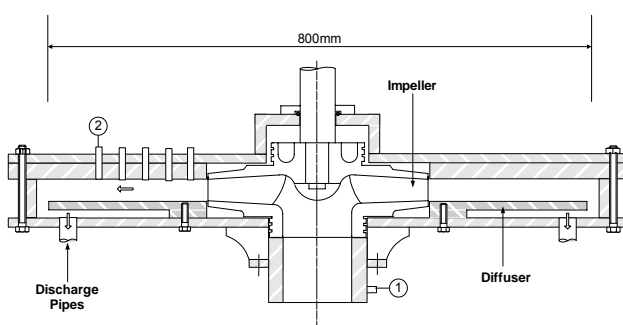

Fig. 1. Cross sectional view of the test section.

The flow-measuring probes "2" can be placed at five radial sections at r=15, 20, 25, 30, 35cm on the diffuser upper wall at the impeller hub side. The location of the pressure transducers on either side of the orifice are selected according to ISO 5167 [11]. The pump was driven by a three phase AC electric motor, the speed of rotation of which can be continuously varied by an inverter. Finally, the flow

rate regulation is obtained by throttling of a butterfly valve installed at the discharge pipe.

Fig. 2. Complete assembly of the experimental apparatus and the model pump.

2.2   Impeller Geometry

The impeller studied in this paper is a radial flow, centrifugal impeller designed and constructed in the Laboratory.

The impeller has 9 two-dimensional (non-twisted) blades with inlet and exit diameter D_1=70 mm, D_2=190 mm, exit width b_2=9 mm and inlet and exit angles β_1=26 deg, β_2=49 deg. The blades follow a single circular arc geometry with a constant blade thickness of s=5mm. The nominal head and flow rate are H=47,5m and Q=62,5m^3/h, respectively, whereas the specific speed is 1311 at n=3000rpm

3   Experimental Results

3.1   Measured and Computed Quantities

The manometric height of the impeller H, is computed from the total energy of the fluid at the inlet and exit of the impeller, points "1" and "2" respectively (Fig. 1):

$$H = H_2 - H_1 = (z_2 + p_2 + \frac{c_2^2}{2g}) - (z_1 + p_1 + \frac{c_1^2}{2g}) \quad (1)$$

where z_2-z_1 is the elevation difference in m, c_2 and c_1 the exit and inlet velocity, and p_2 and p_1 the measured exit and inlet static pressure, respectively. The shaft power N_{shaft} is calculated directly by the human interface program as:

$$N_{shaft} = M_{shaft} \cdot \omega \quad (2)$$

where ω is the angular rotation speed and M_{shaft} the

measured torque. Hence the power transfer to the working fluid is calculated as:

$$N_o = \rho g H Q \qquad (3)$$

where Q is the volume flow rate and ρ the fluid density. In order to extract the characteristic curves of the entire pump, the additional losses shall be properly expressed and taken into account. The mechanical losses at the shaft bearings, along with the disk friction losses shall be taken into account and are estimated to about 90% in total ($\eta_m = 0,9$). No volumetric losses are existed in the present test apparatus (Fig. 2), hence the hydraulic efficiency η_h can be finally defined as:

$$\eta = \eta_m \cdot \eta_h \Rightarrow \eta_h = \frac{N_o}{N_{shaft} \cdot \eta_m} \qquad (4)$$

3.2 Impeller Operation Curves

The experiments were carried out for several constant speeds at 400, 500, 600 and 700rpm. As shown in Fig. 3, the characteristic *H-Q* curves increase with the increase of the rotation speed and are consistent with the affinity laws. A small scattering is observed for high flow rates, due to the instability of the flow and some vibration problems of the test section. Analogous is the behavior of the experimental data for the power in the vertical rotating shaft and the hydraulic efficiency (Fig. 4 and 5, respectively). The maximum obtained efficiency is almost similar for the three series of measurements and about η_h=90%. As, shown in Fig. 5, with the increase of the rotating speed the maximum efficiency is displaced towards higher flow rates, following the theoretical relation:

$$\frac{Q'_k}{Q''_k} = \frac{n'}{n''} \qquad (5)$$

However, the maximum efficiency for the lowest speed (400 rpm) is considerably lower ($\eta_u \approx 82\%$), due to the low Reynolds number and the development of laminar flow regions which cause increased losses to the flow.

3.3 Validation of the Experiments

For the validation of the present measurements available experimental data for the same impeller but with a spiral casing are used. Since that data were taken at 3000rpm, all the present sets of measurements are transformed to this rotation speed. The characteristic curves *H-Q*, η_h-*Q* and N_{shaft}-*Q* for the above two experimental cases are presented and compared in Figs. 6-8.
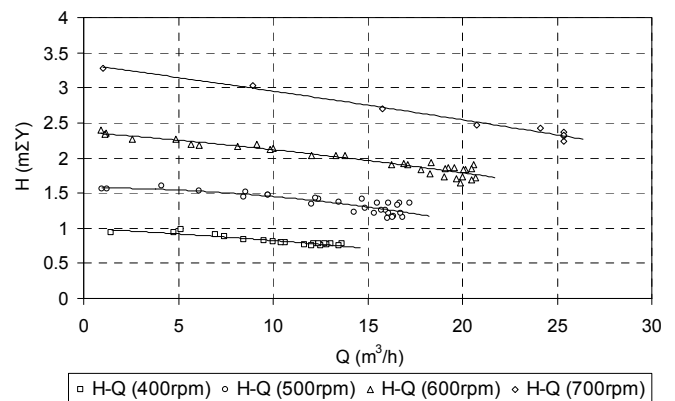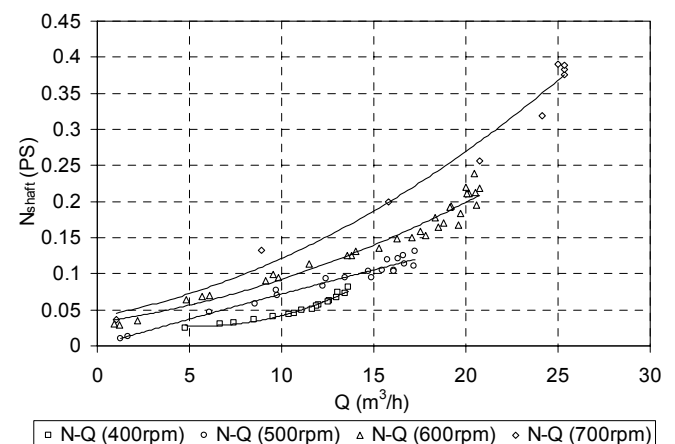

Fig. 3. *H-Q* curves for the measurement data.

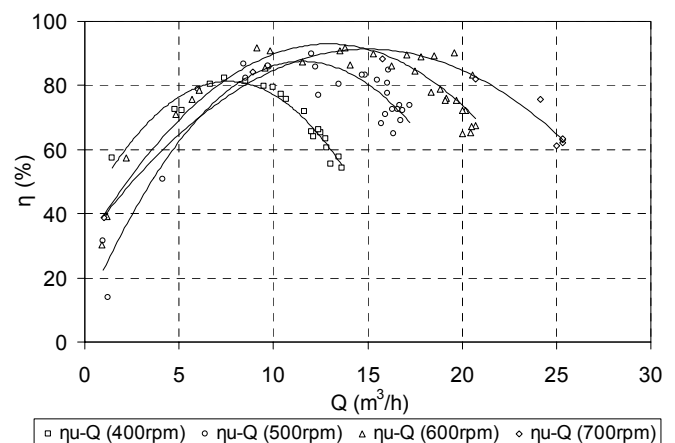Fig. 4. N_{shaft}-*Q* curves for the measurement data.

Fig. 5. η_h-*Q* curves for the measurement data.

The net height and the efficiency of the current test case are, as expected, higher of the respective measurements of the impeller with the spiral casing (Figs. 6 and 7 respectively), because the hydraulic losses in the spiral casing and in the outlet section of the pump are not included in the present

experimental apparatus which contains only the impeller. However, in both cases the electric motor should transmit about the same amount of energy to the impeller for equal flow rates, and this is verified in Fig. 8, where the two power curves almost coincide (η_m is of the same order for both experimental installations).
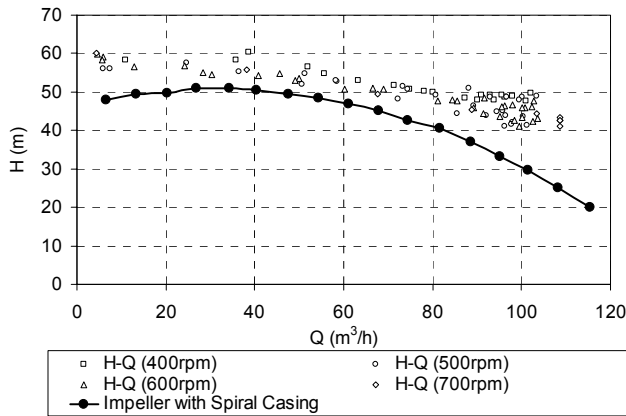

Fig. 6. *H-Q* curves – Comparison with the impeller with the spiral casing.
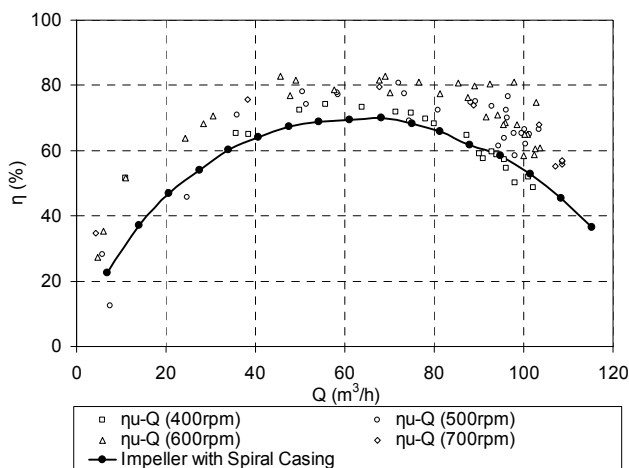

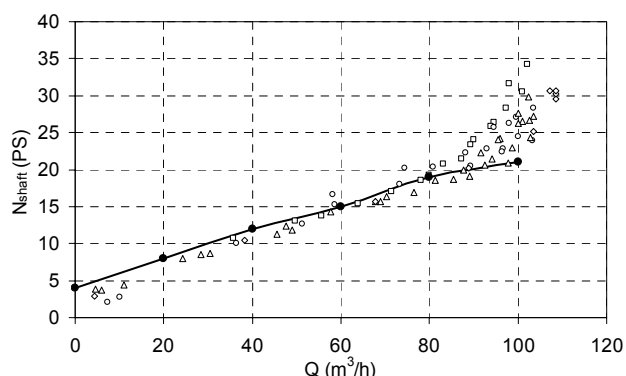Fig. 7. *η -Q* curves – Comparison with the impeller with the spiral casing.

Fig. 8. *N$_{shaft}$-Q* curves – Comparison with the impeller with the spiral casing.

Finally, as shown in Fig. 7, the Best Efficiency Point (BEP) is in the same range for both cases ($Q_k \approx 65 m^3/h$).

4 Numerical Methodology

4.1 Flow Solver

The internal flow is simulated by a single fluid model of a two-dimensional, incompressible, turbulent flow, for which the continuity and momentum equations can be written in the rotating cylindrical coordinate system as follows:

Continuity:

$$\nabla \cdot \vec{w} = 0 \tag{6}$$

Momentum:

$$\vec{w} \cdot \nabla \vec{w} = -2 \vec{\omega} \times \vec{w} + \omega^2 \cdot \vec{r} - \frac{\nabla p}{\rho} + \nu \nabla^2 \vec{w} \tag{7}$$

where p is the fluid pressure, ν is the kinematic viscosity and $\vec{w}$ is the fluid velocity in the rotating system (relative fluid velocity). A Cartesian, unstructured grid system is used for the discretization of the above equations [12], which is generated in a fully automated way and is equipped with an adaptive refinement technique. A pseudo-3D incompressible term is added to the continuity equation to simulate the actual velocity and pressure field in the real 3D domain of the impeller. The main drawback of the Cartesian grid, which is the simulation of irregular boundaries, came over with a "partially blocked cell" technique [10], which makes possible the solution of the grid cells that are crossed by the blade surfaces with almost second order of accuracy. The system of the above equations is numerically solved with the finite volume approach using a preconditioned bi-conjugate gradient (Bi-CG) solver, whereas turbulence is modelled with the standard *k-ε* model. For stability reasons, the algorithm starts from low rotational speed and gradually reaches the nominal speed of 3000rpm.

4.2 Impeller Head and Power Calculations

Using a convergent flow field, the energy gained by the fluid through the impeller, H_{12} is computed from the total energy of the fluid at the impeller inlet and exit periphery, as shown in Fig. 11:

$$H_{12} = H_2 - H_1 = \frac{1}{Q_u} \cdot \int \left(\frac{p_2 - p_1}{\rho g} + \frac{c_2^2 - c_1^2}{2g} \right) dq \tag{8}$$

where c is the absolute velocity of the fluid, Q_u the flow rate through the impeller and g the gravity

acceleration, while the subscripts 1 and 2 denote impeller inlet and exit conditions, respectively (Fig. 9). The integration is approximated by a summation over the radial flow rates δq at all the grid cells facing the inlet or the exit circumference of the impeller. The head given by the impeller, H_u, can be calculated through the torque M_u developed on the blades:

$$N_u = \rho \cdot g \cdot Q_u \cdot H_u = \omega \cdot M_u =$$

$$\omega \cdot \int_{r_1}^{r_2} \left[(\vec{r} \times \vec{n}) \cdot p + (\vec{r} \times \vec{\tau}_w) \cdot \cot \beta \right] \cdot b \cdot dr \qquad (9)$$

where $\vec{n}$ the unit vector normal to the blade surface, $\vec{\tau}_w$ the wall shear stress, β the blade angle and b the impeller width, whereas the integration covers both the pressure side and the suction side of the blade (Fig. 11). Although the simulation is 2-dimensional, the impeller width b is a function of radius r, as in the real impeller.
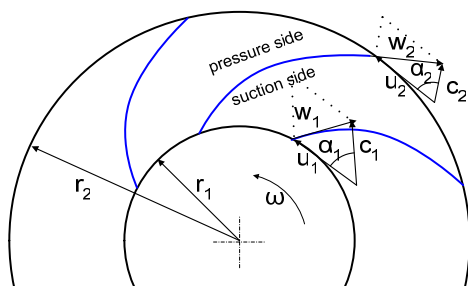

Fig. 9. Sketch of a centrifugal pump impeller.

Hence the impeller head H_u can be computed as:

$$H_u = \frac{\omega \cdot M_u}{\rho \cdot g \cdot Q_u} \qquad (10)$$

and the hydraulic efficiency of the impeller can be finally defined as:

$$\eta_h = \frac{H_{12}}{H_u} \qquad (11)$$

4.3 Comparison between Experimental and Numerical Results

The numerically obtained quantities, net fluid head H_{12}, impeller power N_u and hydraulic efficiency η_h, defined in the previous chapter, correspond to the measured quantities H, $N_{shaft} \cdot \eta_m$ and η_h respectively, as defined in chapter 3.1. Hence, the computed curves H-Q, N_u-Q and η_h-Q of the impeller can be compared with the corresponding

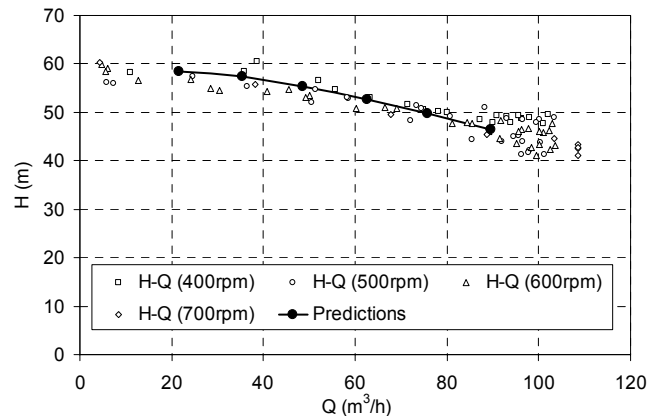measured curves (transformed to 3000rpm). This comparison is shown in Figs. 10, 11 and 12.

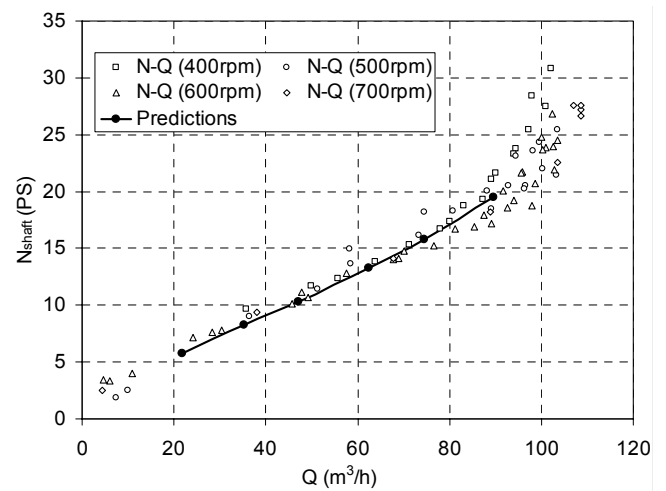Fig. 10. Measured and predicted *H-Q* curves.
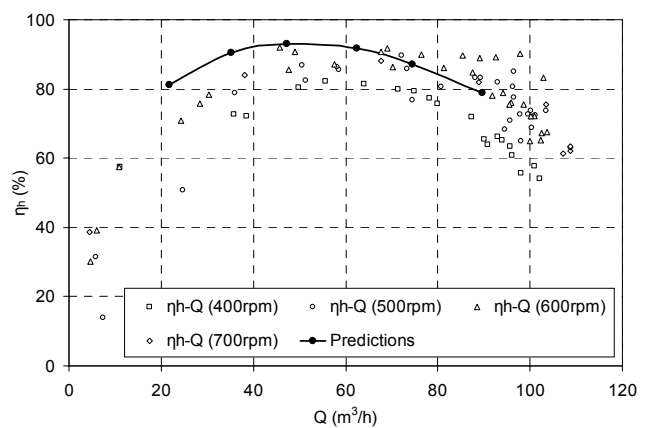

Fig. 11. Measured and predicted *N_shaft-Q* curves.

Fig. 12. Measured and predicted η_h-*Q* curves.

Although the present numerical simulation is 2-dimensional, the agreement with the measurements is quite encouraging. The calculated net fluid head variation approximates very well the corresponding

experimental data and the same is valid for the impeller power curve drawn in Fig. 11. The hydraulic efficiency curve is higher than the measured especially at lower flow rates, below BEP. However, this behavior is expected, because at those flow rates the actual Re number for the experimental rotation speeds (400 to 700rpm) is much reduced and the measured efficiency does not follow the affinity laws.

5 Conclusion

A numerical methodology for the calculation of the flow field in centrifugal pump impellers with 2D curvature is developed and validated against corresponding experimental data taken at a Laboratory test rig.

The flow is calculated using a two dimensional approach in order to achieve a fast simulation and the agreement between the numerical results and the measurements is satisfactory. This is quite encouraging result in order to apply the present numerical model to further flow analysis, as well as, for design optimization purposes in these pump types.

References:
[1] N. Arndt, A.J. Acosta, C.E. Brennen, T.K. Cauughey, Experimental investigation of rotor/stator interaction in a centrifugal pump with several vaned diffusers, *ASME Journal of Turbomachinery*, Vol. 111, 1990, pp. 213-221.

[2] J. Spann, and S. Horgan, The evolution of pump design simulation, *World Pumps*, September 2006, pp. 32-35.

[3] S. Cao, G. Peng, and Z. Yu, Hydrodynamic design of rotodynamic pump impeller for multiphase pumping by combined approach of inverse design and CFD analysis, *ASME Transactions, Journal of Fluids Engineering*, Vol.127, 2005, pp. 330-338.

[4] J. Anagnostopoulos, CFD Analysis and design effects in a radial pump impeller, *WSEAS Trans. on Fluid Mechanics*, Is. 7, Vol. 1, 2006, pp. 763-770.

[5] M. Sinha, J. Katz, *The onset and development of rotating stall within a centrifugal pump with a vaned diffuser*, 3rd ASME/JSME Joint Fluid Engineering Conference, San Francisco, California, July 18-23, 1999.

[6] J. Friedrichs, G. Kosyna, Rotating Cavitation in a Centrifugal Pump Impeller of Low Specific Speed, *ASME J. Fluids Engineering*, Vol. 124, 2002, pp. 101-108.

[7] A. Furukawa, H. Takahara, T. Nakagawa, Y. Ono, Pressure Fluctuation in a Vaned Diffuser Downstream from a Centrifugal Pump Impeller, *Intl. J. of Rotating Machinery*, Vol. 9, 2003, pp. 285-292.

[8] V. Grapsas, M. Mentzos, J. Anagnostopoulos, A. Filios, D. Margaris, D. Papantonis, *Experimental and Computational Study of Radial Flow Pump Impeller*, Proceedings 2st IC-SCCE, Athens, Greece, 5-8 July 2006.

[9] V. Grapsas, J. Anagnostopoulos, D. Papantonis *Hydrodynamic Design of Radial Flow Pump Impeller by Surface Parameterization*, Proceedings 1st IC-EpsMsO, Athens, Greece, 6-9 July, 2005.

[10] J. Anagnostopoulos, *A numerical Simulation Methodology for Hydraulic Turbomachines*, 5th GRACM International Congress on Computational Mechanics, Limassol, Cyprus, 29 June-1 July 2005.

[11] ISO 5167, *Measurement of fluid flow by means of orifice plates, nozzles and venture tubes inserted in circular cross-section conduits running full*, 1980.

[12] J. Anagnostopoulos, Discretization of transport equations on 2D Cartesian unstructured grids using data from remote cells for the convection terms, *Intl. J. for Numerical Methods in Fluids*, Vol. 42, 2003, pp. 297-321.

I.